Distribution Agreement

In presenting this thesis or dissertation as a partial fulfillment of the requirements for an advanced degree from Emory University, I hereby grant to Emory University and its agents the non-exclusive license to archive, make accessible, and display my thesis or dissertation in whole or in part in all forms of media, now or hereafter known, including display on the world wide web. I understand that I may select some access restrictions as part of the online submission of this thesis or dissertation. I retain all ownership rights to the copyright of the thesis or dissertation. I also retain the right to use in future works (such as articles or books) all or part of this thesis or dissertation.

Signature:

_____ _____

Rachel Elizabeth Washington Date

Utilizing Multireference Driven Similarity Renormalization Group to Study 3d Transition Metal Atoms and Hydrides

By

Rachel Elizabeth Washington

Master of Science

Chemistry

_____

Dr. Francesco A. Evangelista, Ph.D
Advisor

_____

Dr. Joel M. Bowman, Ph.D
Committee Member

_____

Dr. Raphael F. Ribeiro, Ph.D
Committee Member

Accepted:

_____

Kimberly Jacob Arriola, Ph.D, MPH
Dean of the James T. Laney School of Graduate Studies

_____

Date

Utilizing Multireference Driven Similarity Renormalization Group to Study 3d Transition Metal Atoms and Hydrides

By

Rachel Elizabeth Washington
B.A., Willamette University, 2019

Advisor: Dr. Francesco A. Evangelista, Ph.D

An abstract of
A thesis submitted to the Faculty of the James T. Laney School of Graduate Studies of Emory University in partial fulfillment of the requirements for the degree of
Master of Science
in Chemistry
2021

Abstract

Transition metal complexes play a fundamental role in biological processes and chemical catalysis; however, they remain difficult to study computationally. Computational challenges arise due to the presence of strong and weak electron correlation and the competition between states of different spin multiplicity. However, most computational techniques do not adequately capture both forms of electron correlation. Most multireference techniques accurately capture strong electron correlation while most single reference techniques efficiently describe weak electron correlation. The primary difficulty, in studying 3d transition metal compounds computationally is to capture both forms of electron correlation within the calculation. Presented here is the utilization of the multireference driven similarity renormalization group (MRDSRG) method to benchmark 3d transition metal hydrides. MRDSRG can account for strong electron correlation through multiple Slater determinants and weak electron correlation using a sliding parameter to control the extent the Hamiltonian is block-diagonalized. This thesis presents the analysis of several 3d transition metal hydrides, and the first computation of the ionization energies of 3d transition metals with MRDSRG, with a comparison to other computational techniques.

Utilizing Multireference Driven Similarity Renormalization Group to Study 3d Transition Metal Atoms and Hydrides

By

Rachel Elizabeth Washington
B.A., Willamette University, 2019

Advisor: Dr. Francesco A. Evangelista, Ph.D

A thesis submitted to the Faculty of the James T. Laney School of Graduate Studies of Emory University in partial fulfillment of the requirements for the degree of
Master of Science
in Chemistry
2021

Table of Contents

List of Figures

List of Tables

Chapter 1 Introduction

1.1) Introduction

Transition metal complexes provide the building blocks for large transition metal complexes that play an essential role in several critical biological processes and chemical applications. In particular, transition metal complexes play a significant role in the development of catalysts for industrial processes,[1] solar cells,[2] and the delivery of pharmaceuticals in the body.[3] Despite, the importance of transition metals in everyday life they remain difficult to understand computationally.

Challenges in studying transition metal complexes computationally arises from the partially occupied d-shell. When partially occupied, the 5 atomic d orbitals lead to multiple possible electron configurations for a transition metal atom. For example, Figure 1 showcases two possible electron configurations with different spin multiplicities (m_s) for a cobalt (Co) atom. The electron configurations are both open-shell, and thus, lead to several more possible electron configurations for each spin multiplicity than shown in Figure 1. For, m_s=4 there are 10 possible electron configurations with 3 alpha electrons, as shown in Figure 2. The multiple electron configurations cause several energy states to be degenerate or near-degenerate. Energetic states close in energy can cause computational

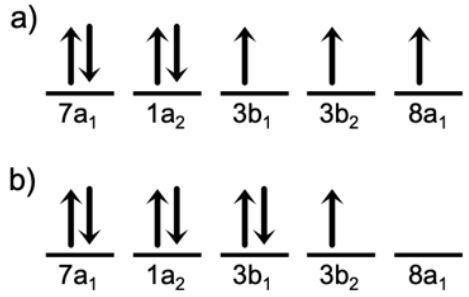

Figure 1. The 3d orbital for two electron configurations of a cobalt atom. The m_s=4 for configuration a and m_s=2 for configuration b.

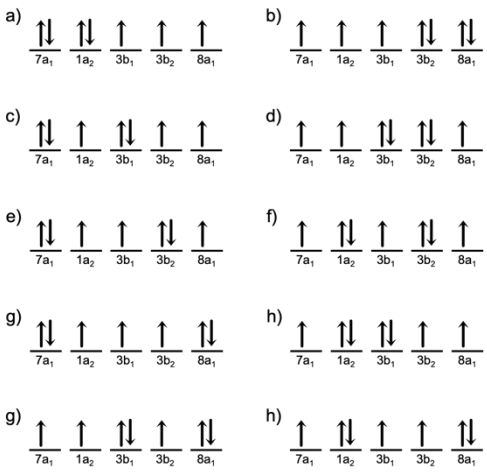

Figure 2. The 3d orbital of 10 different electron configurations of a Co atom with m_s=4, where the spin of electrons in singly occupied orbitals is neglected.

techniques to converge on the incorrect electronic configuration and the wrong identification of the ground state. Figure 2 reduces the simplicity of the chemical systems analyzed in this project. Accurate calculations cannot just consider a single spin state and thus, significantly increases the possible electron configurations for a singular Co atom. The complexity of the problem increases further when electron configurations with m_s=2 are considered.

Additionally, analyzing 3d transition metal hydrides adds further difficult due to the mixing of atomic orbitals to form of molecular orbitals between the 3d transition metal and the hydrogen atom. Therefore, you can see the scale of the systems studied here as more electron configurations must be considered then the Co atom described in Figures 1 and 2. The separation energy between states of different multiplicities must also be evaluated. For example, Kulik and coworkers studied the energy difference between MnH $^5\Sigma^+$ and MnH $^7\Sigma^+$ and found the septet state to be the lowest energy state.[4] The expected lowest energy state would be the quintet state since, more electrons are not paired together, decreasing the repulsion energy between electrons. However, the interaction energy between the molecular orbitals is significantly less between the anti-bonding 4s orbital and the 3d orbitals than expected, and the anti-bonding 4s orbital has very little anti-bonding character. This leads to the repulsive energy between electrons having less of an energetically stabilizing effect than the interaction energy, and as a result the septet state to be the unexpected ground state. The MnH $^7\Sigma^+$ ground state was also confirmed experimentally via laser spectroscopy.[5]

The computational analysis of 3d transition metals and transition metal hydrides was performed using multireference driven similarity renormalization group with second order and third order perturbation theory (MRDSRG-PT2 and MRDSRG-PT3). The following sections will describe the computational methods utilized. In addition, the computational techniques that are compared to the acquired data and the corresponding studies are also evaluated. A complete set of spectroscopic constants for the following molecules - ScH $^1\Sigma^+$, TiH $^4\Phi$, MnH $^5\Sigma^+$, MnH $^7\Sigma^+$, and ZnH $^2\Sigma^+$ were obtained and analyzed with MRDSRG-PT3. Ionization energies for all 3d

transition metals were evaluated with MRDSRG-PT2 and MRDSRG-PT3. An analysis of the energy splitting obtained with MRDSRG-PT3 between MnH $^5\Sigma^+$ and MnH $^7\Sigma^+$ was studied. Lastly, the equilibrium bond lengths for ScH $^1\Sigma^+$, TiH $^4\Phi$, CrH $^4\Sigma^+$, CrH $^6\Sigma^+$, MnH $^5\Sigma^+$, MnH $^7\Sigma^+$, FeH $^4\Delta$, FeH $^6\Delta$, CoH $^3\Phi$, CuH $^1\Sigma^+$, and ZnH $^2\Sigma^+$ were obtained.

1.2) **The Schrödinger Equation**

The basis of quantum chemistry is to solve the full nonrelativistic time-independent Schrödinger equation and obtain the energy for a chemical system of interest. The Schrödinger equation is defined as,

$$\widehat{H}\Psi = E\Psi \tag{1}$$

where $\widehat{H}$ is the Hamiltonian operator, Ψ is the molecular wave function, and E is the energy. For a system with M nuclei and N electrons, the full Hamiltonian is,

$$\widehat{H} = -\sum_{i=1}^{N}\frac{1}{2}\nabla_i^2 - \sum_{A=1}^{M}\frac{1}{2M_A}\nabla_A^2 - \sum_{i=1}^{N}\sum_{A=1}^{M}\frac{Z_A}{r_{iA}} + \sum_{i=1}^{N}\sum_{j>i}^{N}\frac{1}{r_{ij}} + \sum_{A=1}^{M}\sum_{B>A}^{M}\frac{Z_A Z_B}{R_{AB}} \tag{2}$$

with the indices A and B used to label nuclei and the indices i and j for the electrons. Derivatives with respect to the A-th nucleus and the i-th electron enters via the Laplacian operators, ∇_A^2 and ∇_i^2 respectively; these two terms account for the kinetic energy. The ratio between the mass of the A-th nucleus and an electron, the distance between the i-th electron and the A-th nucleus, the atomic number of the A-th nucleus, the distance between the i-th electron, and the distance between A-th and B-th nucleus are defined as M_A, r_{iA}, Z_A, r_{ij}, and R_{AB} sequentially. The attraction of the negatively charged electrons and positively charge nuclei (Coulomb attractions) is accounted for in the third term of the Hamiltonian. The repulsion between negatively charged electrons is considered in the fourth term, while the fifth term represents the repulsion between the nuclei.

A challenge of solving the Schrödinger equation arises from the coupling of electrons and nuclei within the Hamiltonian.[6] When analyzing chemical systems with 3d transition metals a minimum of 21 electrons for Scandium (Sc) must be considered in the Hamiltonian. To simplify the Hamiltonian the second and fifth term of Equation 2 is disregarded, since the mass of nuclei are significantly greater than the mass of electrons. Under this assumption, the nuclei move much slower than electrons, allowing to factorize the nuclei and the electron wavefunctions. Then the electrons satisfy a Schrödinger equation similar to Equation 1 with the Hamiltonian defined as,

$$\widehat{H} = -\sum_{i=1}^{N} \frac{1}{2} \nabla_i^2 - \sum_{i=1}^{N} \sum_{A=1}^{M} \frac{Z_A}{r_{iA}} + \sum_{i=1}^{N} \sum_{j>i}^{N} \frac{1}{r_{ij}} \tag{3}$$

This simplification is referred to as the Born-Oppenheimer Approximation (BO Approximation). However, the errors due to the BO Approximation are largely negligible when completing calculations on the equilibrium properties of transition metals.

1.3) **Full-Configuration Interaction**

Additionally, solving the Schrödinger equation requires a wavefunction that describes the chemical system of interest. Capturing every possible electron configuration for the transition metal system of interest is the primary concern when building a wavefunction. This is accomplished by enumerating determinants for all electron configurations.

Slater determinants are built from a basis of one-electron wavefunctions or spin orbitals, where each spin orbital describes a single electron. A wavefunction for a single electron is comprised of two components - a spatial orbital $\phi_i(\vec{r})$ and a spin component $\alpha(\omega)$ or $\beta(\omega)$ with spin variable ω. The spatial orbital refers to the position of an electron i at $\vec{r}$. Furthermore, when normalized spatial orbitals are used, the probability of finding the electron at position $\vec{r}$ within the volume of d$\vec{r}$ is given by $|\phi_i(\vec{r})|^2$. Furthermore, the spatial orbitals are assumed to be orthonormal.

The other component of a spin orbital is the spin component that can either be spin-up ($\alpha(\omega)$) or spin-down ($\beta(\omega)$). Therefore, a spin orbital for an electron i is defined as a product of the spin component and spatial orbital to form a function of variable $\mathbf{x} \equiv (\vec{r}, \omega)$ (Equation 4).

$$\psi(\mathbf{x}) = \begin{cases} \phi_i(\vec{r})\alpha(\omega) \\ \phi_i(\vec{r})\beta(\omega) \end{cases} \tag{4}$$

A basis of spin orbitals built from a finite set of $\mathbf{M}$ spatial orbitals such that $\mathrm{i} \in 1, 2, \ldots, \mathbf{M}$ given a basis set of $2\mathbf{M}$ orthonormal spin orbitals, is defined by

$$\begin{aligned} \psi_{2i-1}(\mathbf{x}) &= \phi_i(\vec{r})\alpha(\omega) \\ \psi_{2i}(\mathbf{x}) &= \phi_i(\vec{r})\beta(\omega) \end{aligned} \tag{5}$$

A wavefunction of $\mathbf{N}$ electrons (Equation 6) can be formed from a basis of $2\mathbf{M}$ spin orbitals (Equation 5) as an antisymmetric product of single electron wavefunctions.

$$\Phi(x_1, x_2, \cdots, x_{\mathbf{N}}) \tag{6}$$

As an example, we will consider a two-electron system for electron x_1 and x_2, then the wavefunction will be described by Equation 7.

$$\Phi(x_1, x_2) \tag{7}$$

The wavefunction in Equation 7 can be expanded in the complete spin orbital basis to form Equation 8.

$$\Phi(x_1, x_2) = \sum_{rq} C_{rq}\psi_r(x_1)\psi_q(x_2) \tag{8}$$

Where, ψ_r and ψ_q represent spin orbitals the r-th and q-th molecular orbitals. However, for Equation 8 to correctly describe a two-electron system the Pauli Exclusion Principle must be satisfied. However, Equation 8 must satisfy the Pauli Exclusion Principle for fermions; since, electrons are fermions.

For fermions to meet the Pauli Exclusion principle, the total wavefunction must be anti-symmetric with respect to the interchange (Equation 9):

$$\Phi(x_1, x_2) = -\Phi(x_2, x_1) \tag{9}$$

Thus, to meet this requirement we can examine two possibilities. For electron x_1 to occupy the ψ_r spin orbital while electron x_2 occupies the ψ_q spin orbital (Equation 10). Additionally, electron x_1 to occupy the ψ_q spin orbital while electron x_2 occupies the ψ_r spin orbital (Equation 11).

$$\Phi(x_1, x_2) = \psi_r(x_1)\psi_q(x_2) \tag{10}$$

$$\Phi(x_2, x_1) = \psi_r(x_2)\psi_q(x_1) \tag{11}$$

To build a wavefunction that satisfies Pauli Principle (Equation 9) the wavefunction should be written as a linear combination of Equation 10 and 11 to obtain Equation 12.

$$\Phi(x_1, x_2) = \frac{1}{\sqrt{2!}}\left[\psi_r(x_1)\psi_q(x_2) - \psi_r(x_2)\psi_q(x_1)\right] \tag{12}$$

In Equation 12 a normalization factor of is applied. Additionally, Equation 12 can be represented as a determinant (Equation 13).

$$\Phi(x_1, x_2) = \frac{1}{\sqrt{2!}}\begin{vmatrix} \psi_r(x_1) & \psi_r(x_2) \\ \psi_q(x_1) & \psi_q(x_2) \end{vmatrix} \tag{13}$$

Equation 13 defines a Slater determinant for the two-electron system and this definition can be expanded to a system of $2\mathbf{M}$ spin orbitals and $\mathbf{N}$ electrons (Equation 14):

$$\Phi_{r,q,\cdots M}(x_1, x_2, \cdots, x_{\mathbf{N}}) = \frac{1}{\sqrt{\mathbf{N}!}}\begin{vmatrix} \psi_r(x_1) & \cdots & \psi_r(x_{\mathbf{N}}) \\ \vdots & \ddots & \vdots \\ \psi_{\mathbf{M}}(x_1) & \cdots & \psi_{\mathbf{M}}(x_{\mathbf{N}}) \end{vmatrix} \tag{14}$$

Slater determinants are abbreviated without electron labels as $\left|\Phi_{r,q,\cdots\mathbf{M}}\right\rangle = \left|\psi_r\psi_q\cdots\psi_{\mathbf{M}}\right\rangle$ for convenience. Thus, the wavefunction for a transition metal system can be fully described by Equation 15.

$$|\Phi\rangle = \sum_{i_1<i_2<\cdots<i_{\mathbf{N}}}^{2\mathbf{M}} c_{i_1,i_2,\cdots i_{\mathbf{N}}}\left|\psi_r\psi_q\cdots\psi_{\mathbf{M}}\right\rangle \tag{15}$$

Where, $c_{i_1,i_2,\cdots i_{\mathbf{N}}}$ are the resulting coefficients for each determinant. For example, if we were to examine Figure 2 and compose Slater determinants for the wavefunction of the Co atom. There will be at least 10 Slater determinants for each possible configuration and will have a likelihood for the Co atom to be in that electron configuration. The coefficients, $c_{i_1,i_2,\cdots i_{\mathbf{N}}}$ describe how much each Slater determinant will contribute to the wavefunction.

This method of describing the wavefunction is the Full-Configuration Interaction (FCI). When the full-nonrelativistic Schrödinger equation is applied to the FCI wavefunction, the exact energy is obtained. However, the significant issue in using FCI to study transition metal chemistry is one of scale. As more Slater determinants are needed to describe an atom or molecule computation cost increases exponentially with $2\mathbf{M}$ spin orbitals and $\mathbf{N}$ electrons.[7]

1.4) **Hartree-Fock Theory and other Single-Reference Techniques**

Hartree-Fock theory and other single-reference techniques assume wavefunctions comprised of a singular Slater determinant. The goal is to build a wavefunction of the most optimum spin orbitals (Equation 16).

$$|\Phi_0\rangle = |\psi_1, \psi_2, \psi_3, \cdots, \psi_N\rangle \tag{16}$$

Then using the Hamiltonian defined in Equation 3 and Equation 16 the energy can be obtained. Additional, single reference techniques use the HF wavefunction as a reference by replacing portions of Equation 16 to approximate the FCI wavefunction. These techniques include Couple Cluster theory with singles, doubles, and triples (CCSD(T)) and second order Møller-Plesset perturbation theory (MP2).

These techniques have been utilized with some success to analyze transition metal chemistry. Specifically, the CCSD(T) method (or coupled-cluster theory with singles, doubles, and perturbative triple clusters) has been hailed as the “gold standard” of computational techniques and has even been utilized to challenge experimentally obtained data.[8] Unfortunately, CCSD(T) is not as accurate as some DFT functionals in determining the

dissociation energy of transition metal hydrides which was demonstrated by Moltved and Kepp.[9] Additionally, several studies have determined that CCSD(T) is not an effective singular benchmark when transition metals are involved.[9–11]

1.5) **Density Functional Theory**

Another technique utilized to study transition metal chemistry is Density Functional Theory (DFT). This technique uses the electron density $\rho(r)$ to describe an $\mathbf{N}$ electron system $\psi(x_1, x_2, \cdots, x_{\mathbf{N}})$ rather than an expansion in terms of Slater determinants. This reduces the computational scaling of solving for the energy to wavefunction methods. Generally, the energy can be obtained via functionals of the kinetic energy (T), the nuclear-electron potential energy (V_{ex}), and the electron-electron repulsion energy (V_{ee}).

DFT techniques have been utilized to study transition metal complexes with varied success. However, this method neglects strong electron correlation present in the bonds of transition metal complexes. Specifically, conventional DFT does not obtain accurate electronic structure properties for small transition metal complexes (such as hydrides, and carbides) due to the strong electron correlation present in the transition metal-containing bonds. On the other hand, modified DFT has been created to address strongly correlated electrons. Modified DFT approaches include Kulik and Marzari that use a correction factor (U) to account for strong electron correlation, also called the Hubbard-model approach or DFT+U.[4] Another approach, was developed by Johnson and Becke [12] that implemented the B13 functional to account for strong electron correlation in real space and determine spin-restricted dissociation limits of molecular bonds. These approaches can be successful; for example, the B13 functional was able to determine the dissociation energy of copper diatomic (Cu2) within <1 kcal/mol (or 0.01 eV) of the experimental value.[12] However, Aoto and coworkers [10] completed a successful benchmark of several transition metal compounds and pinpoint the major disadvantage of all DFT approaches - correction factors and functionals can fail in unexpected cases, and DFT does not provide a good systematic hierarchy of approximations.[10]

1.6) **Multireference Techniques**

Complete Active Space Self-Consistent Field Method

Multireference techniques were employed in this report to study 3d transition metal hydrides and the ionization energies of 3d transition metal hydrides. An initial HF calculation was completed as an initial starting point for all calculations followed by a series of multireference techniques. The first multireference calculation performed used Complete Active Space Self-Consistent Field Method (CASSCF). The procedure utilized follows Hohenstein et al.[13] but accounts for non-redundant rotations using the approach of Chaban et al.[14] and active-active rotations using a two-step optimization from Keplin et al.[13]

$$|\Psi_{CASSCF}\rangle = \sum_{I} C_I |\Phi_I\rangle \tag{17}$$

$$E_{CASSCF} = \min_{C_I,\{\psi_i\}} \langle \Psi_{CASSCF} | \hat{H} | \Psi_{CASSCF} \rangle \tag{18}$$

The wavefunction is defined by Equation 17 for CASSCF and is formed from the FCI wavefunction described in Section 1.3. Therefore, Φ_I will be the Slater determinants and C_I will be the corresponding coefficients. Then the energies are obtained by solving the Hamiltonian in Equation 18.

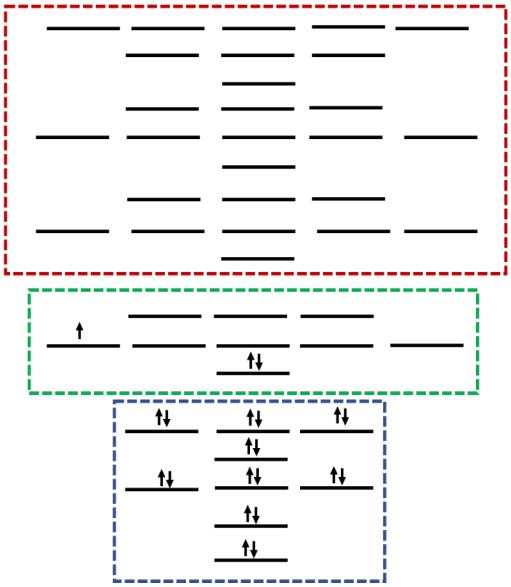

Figure 3. Representation of the orbital division CASSCF method using Scandium Atom with a full-valence active space. The virtual, active, and core orbitals are encompassed by red, green and blue respectively.

Unlike the FCI wavefunction, the CASSCF wavefunction uses a finite selection of spin orbitals in Equation 17. The spin orbitals are divided into three blocks – occupied, active, and virtual (Figure 3). How the orbitals are represented within the wavefunction (Equation 2) are described by the

following descriptions. The virtual orbitals are not included since they are high in energy, and do not alter the description of the chemical system. The occupied orbitals are the lowest in energy and will always remain doubly occupied within the CASSCF wavefunction. The active orbitals are the orbitals that play an active role and will have varying occupations. A benefit of the CASSCF method is that all possible electronic states within the active space can be accounted. However, the disadvantage is that the selection of the active space plays an important role in CASSCF calculations.

Atomic Valence Active Space

To generate the appropriate active space with consistent orbital ordering AVAS (atomic valence active space) was utilized. Sayfutyarova and coworkers developed AVAS to improve the consistency of multireference calculations.[15] Using AVAS to generate consistent active spaces avoids the vulnerabilities associated with user-chosen active spaces which significantly increases the time required to determine a active space and can lead to a poor quality in results. In addition, the energy ordering of orbitals can be inconsistent at different bond distances in CASSCF calculations leading to inaccurate results due to a calculation to converging on an incorrect energy state.

To complete AVAS, the user provides a specified set of atomic orbitals for the active space. For example, calculations completed here for 3d transition metal hydrides use the 4s, 4p, and 3d atomic orbitals of the 3d transition metal and the 1s atomic orbital of hydrogen atom for the construction of the active space. While the active space for the 3d transition metal atoms includes the 4s, 4p, and 3d atomic orbitals. The first step for an AVAS calculation is to obtain the occupied and virtual molecular orbitals by completing a HF calculation. The occupied molecular orbitals are defined by indices i and j, while virtual molecular orbitals by a and b. Next, the user specified target atomic orbitals are defined via the MINAO[16] basis set to form a matrix of the targeted atomic orbitals, $\mathbf{A}$. Then the overlap matrices between the occupied

orbitals and $\mathrm{span}(\mathbf{A})$ (Equation 19), as well as between the virtual orbitals and $\mathrm{span}(\mathbf{A})$ (Equation 20) are formed.

$$S_{ij} = \langle i | \hat{P}_{\mu v} | j \rangle \tag{19}$$

$$\bar{S}_{ab} = \langle a | \hat{P}_{\mu v} | b \rangle \tag{20}$$

the projector matrix is defined as,

$$\hat{P}_{\mu v} = \sum_{pq} \langle \mu | p \rangle (\mathbf{A}^{-1}) \langle q | v \rangle$$

The projector matrix within Equations 19 and 20 contains the user specified target atomic orbitals. Next, the overlap matrices (Equations 19 and 20) are diagonalized to yield to the molecular orbitals that are also within the user specified atomic orbitals. The eigenvectors ascertained from the diagonalization of Equations 19 and 20 represent the molecular orbitals to build the active space for the occupied and virtual spaces respectively. Thus, forming the active space with this technique ensures that the chosen orbitals for multireference methods are consistent in ordering and within the user specified target atomic orbitals. Furthermore, to ensure high quality active space selection, AVAS was performed prior to every CASSCF calculation completed in this report.

Perturbative Multireference Driven Similarity Renormalization Group

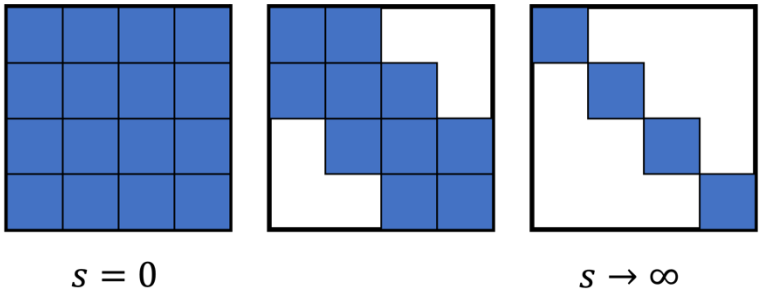

Figure 4. A visual representation of the gradual block diagonalization of the Hamiltonian controlled by the flow parameter *s*.

The computational method of analysis in this study is multireference driven similarity renormalization group (or MRDSRG). MRDSRG is different than other multireference techniques since it encapsulates the weak electron correlation with a flow parameter (s) within the Hamiltonian and strong electron correlation using multiple Slater determinants. However, most multireference techniques only capture strong electron correlation making MRDSRG unique (the concept of electron correlation is further explored in Section 1.7.[17] An aim of this study is to determine the efficacy of the MRDSRG technique in the analysis of 3d transition metal hydrides and ionization energies.

$$\Omega: H \to H^{eff} = \Omega^{-1} H \Omega \tag{21}$$

$$\Omega = e^{\hat{A}(s)} = e^{\hat{T}(s) - \hat{T}^{\dagger}(s)} \tag{22}$$

$$\left[H^{eff}\right]_N = \hat{R}(s) \tag{23}$$

DSRG is built upon a similar foundation to unitary coupled-cluster techniques where a continuous similarity transformation of the bare Hamiltonian is completed.[18] The transformation occurs via a wave operator (Ω) and follows Equation 21. For DSRG, Ω accounts for weak electron correlation and is described by Equation 22. The flow parameter (s) is chosen such that $s \in [0, \infty)$ and Ω utilizes the unitary coupled-cluster operator $\hat{T}(s) - \hat{T}^{\dagger}(s)$ which can be solved as a set of nonlinear equations using the source operator $\hat{R}(s)$ and includes the non-diagonal

terms N (Equation 23). This approach succeeds where others fail due to the gradual block-diagonalization of the Hamiltonian controlled by s.

Figure 4 showcases how s impacts the Hamiltonian. When $s = 0$ the Hamiltonian is not diagonalized and has no electron correlation introduced. As s is increased a "sweet spot" is reached and the Hamiltonian is in the form of a banded structure. At this "sweet spot" the interference of energy denominators between degenerate or near degenerate states commonly referred to as intruders are removed.[17] The consideration of intruders is important since they lead to unintentional spikes in the potential energy curve and affect the quality of spectroscopic data. Further correlation is accounted for in a correlated wavefunction. As $s \to \infty$ the Hamiltonian becomes perfectly diagonalized. It could be assumed that picking a large s value would be beneficial as a diagonalized Hamiltonian would have the energies as the eigenvalues. However, when the s value is too large intruder states are re-introduced and convergence of the DSRG procedure is not possible.

$$|\Psi_0\rangle = \sum_{\mu=1}^{d} c_\mu |\Phi^\mu\rangle \tag{24}$$

$$E(s) = \langle \Psi_0 | H^{eff} | \Psi_0 \rangle \tag{25}$$

The reference wavefunction for MRDSRG is formed from the FCI wavefunction like the CASSCF procedure (Equation 24) and is similarly divided into the 3 orbital spaces in Figure 4. Then the MRSRG energy is calculated via Equation 25. The 3d transition metal atoms and hydrides require a large basis to perform accurate calculations.[19] In addition, MRDSRG computational cost increases with basis size.[17] Thus, MRDSRG with low-order perturbation theory (PT2 and PT3) was employed for all calculations to reduce computational costs. The process of determining the energy for MRDSRG-PT2 and MRDSRG-PT3 (Equation 26 and 27

respectively) is like MRDSRG except an order-order expansion of the wavefunction (Equation 24), the source operator $\hat{R}(s)$ (Equation 23), and the Hamiltonian (Equation 25).

$$E^{(2)} = \langle \Psi_0 | [H^{(1)} + \bar{H}^{(1)}, \hat{T}^{(1)}] | \Psi_0 \rangle \tag{26}$$

where,

$$\bar{H}^{(1)} = H^{(1)} + [\hat{H}^{(0)}, \hat{A}^{(1)}] = H^{(1)} + [\hat{R}^{(1)}(s)]_N$$

$$E^{(3)} = \langle \Psi_0 | [\bar{H}^{(1)}, \hat{T}^{(2)}] | \Psi_0 \rangle + \langle \Psi_0 | [\bar{H}^{(2)}, \hat{T}^{(1)}] | \Psi_0 \rangle \tag{27}$$

and $\bar{H}^{(2)}$ is defined as,

$$\bar{H}^{(2)} = [\hat{H}^{(0)}, \hat{A}^{(2)}] + [\hat{H}^{(1)}, \hat{A}^{(1)}] + \frac{1}{2}\left[[\hat{R}^{(1)}(s)]_N, \hat{A}^{(1)}\right]$$

1.7) **Electron Correlation**

The interactions between the electrons causes a significant challenge in studying transition metals atoms and molecules computationally. These interactions are called electron correlation and can be quantified by the electron correlation energy. A formal definition of the electron correlation energy is the difference between the FCI energy or the exact energy and the HF energy (Equation 28).

$$E_{\text{corr}} = E_{\text{FCI}} - E_{\text{HF}} \tag{28}$$

Where, E_{corr} is the electron correlation energy, E_{FCI} is the FCI energy, and the E_{HF} is the HF energy.

A significant challenge in studying transition metal chemistry computationally is the electron correlation present. This becomes apparent when considering the mean-field approximation cannot sufficiently describe transition metals, due to strong interactions amount the d-shell electrons. The d-shell leads to several low-lying energy

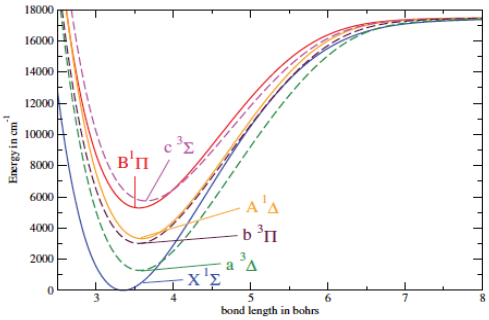

Figure 5. Potential energy curves for ScH generated by Lodi et al. using MRCI.

states that are degenerate or near-degenerate, multiple multiplicities for the same molecule, and a generally open-shell electronic structure. These qualities lead to higher electron interaction and thus, a larger electron correlation energy. We can use scandium hydride (ScH) studied by Lodi and coworkers[20] which used a multireference method, multi-reference configuration interaction (MRCI) to successfully plot potential energy curves for 6 states of ScH; resulting in, a total of six low-lying electronic states predicted computationally with 3 – triplet states and 3 – singlet states (Figure 5). We can further divide the electron correlation present here and in all systems into strong/nondynamical and weak/dynamical correlation.

Strong/nondynamical correlation arises due to the interaction between energy states that are degenerate or near-degenerate and is generally observed when analyzing bond-breaking processes, open-shell systems and excited states. In the example of ScH, we can determine that the ground state $X^1\Sigma^+$ and the first excited state $a^3\Delta$ are near-degenerate, reflecting the degeneracy of the d orbitals. In this case the ground state is closed-shell but due to the open d-shell ScH has an open-shell state causing strong electron correlation.

Nondynamical correlation is not captured in methods that are built on a single determinant (such as HF) and a multi-reference method built on multiple determinants (such as MRCI) is necessary. This can be shown using a simple two electron system such as dissociation of hydrogen gas (H_2).[7] Examining the bond breaking process of the H_2 molecule we can determine there will be two possible states as H_2 dissociates which are $H\uparrow\cdots H\downarrow$ and $H\downarrow\cdots H\uparrow$ where the alpha and beta electrons are flipped between hydrogens (Figure 6). The exact or the FCI energy is calculated using a linear combination of the two covalent determinants for the wavefunction. However, HF includes ionic contributions which causes the energy to be higher than the exact energy and the strong electron correlation to not be accounted for. HF assumes that each hydrogen atom has a probability of 50%, 25%, and 25% to have a charge of 0, +1, and -1 respectively. Thus, the HF wavefunction would be weighted to include two covalent configurations ($H\cdots H$) and two ionic contributions ($H^+\cdots H^-$, $H^-\cdots H^+$). The ionic contributions

should not be included in the HF wavefunction because they are unfavorable due to the Coulomb repulsion between the positively and negatively charged hydrogen atoms (Figure 7). This example demonstrates why the HF method along with other single reference methods to be unable to capture nondynamical correlation due to the inclusion of energetically unfavorable ionic contributions.

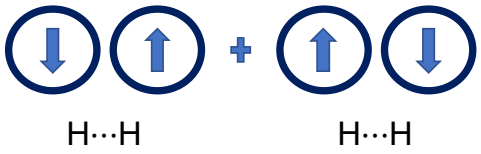

Figure 6. Covalent contributions in the FCI/multi-reference wavefunction for H_2

Figure 7. Covalent and ionic contributions in the HF wavefunction for H_2

On the other hand, weak/dynamical electron correlation is generally not captured by multireference techniques. Weak electron correlation is caused by short-range Coulomb interactions and long-range London dispersion forces. These forces are often seen at the end of a potential energy curve. Most multireference techniques do not account for weak electron since it generally occurs when there are small contributions of excited determinants in the wavefunction.[7] Including these effects can be computationally expensive and thus many single-reference methods such as coupled cluster theory with singles, doubles and triples (CCSD(T)) are able to capture weak-electron correlation in a cost-effective manner. With any computational technique, the primary difficulty with analyzing transition metals is capturing both forms of electron correlation in an effective manner.

Chapter 2 Perturbative MRDSRG Calculations

2.1) Introduction

Completed calculations for a selection of 3d transition metal hydrides and the ionization energy of every 3d transition metal are presented here. Chapter 1 includes the theory behind the multireference methods utilized. As described in the previous chapter the primary difficulty of studying transition metals computationally is the weak and strong electron correlation present. Furthermore, most computational methods only account for either weak or strong electron correlation.

Previous analysis for transition metals has utilized a myriad of methods for single reference techniques from CCSD(T) by Moltved and Kepp,[9] to modified DFT approaches by Kulik and Marzari,[4] and Johnson and Becke.[21] Despite the success in modified DFT approaches, they can fail in unexpected cases due to how the approximations to account for strong electron correlation are implemented.[10] Furthermore, preceding studies that analyzed the effectiveness of CCSD(T) in benchmarking transition metal compounds found it was not an adequate singular benchmark when transition metals are involved.[9–11]

The utilization of multireference techniques completed by Lodi et al.[20] and Aoto et al.[10] were successful in analyzing transition metal complexes. Lodi and coworkers were able to successfully plot several potential energy curves for ScH using MRCI. Additionally, Aoto and colleagues were able to successfully benchmark 60 transition metal diatomics internally contracted multireference CCSD(T) (icMRCCSD(T)).[10] Although these techniques have effectively been able to ascertain results for transition metal complexes, MRDSRG includes a refined consideration of intruders. Thus, the utilization of MRDSRG could provide new insight to the treatment of transition metal complexes.

However since MRDSRG was developed by our research group[17] a systematic study of its efficacy in the analysis of transition metals has not been completed. The goal of this analysis

is to utilize MRDSRG to benchmark 3d transition metal hydrides and the first ionization energies. Presented here are results for the first ionization energy for all 10, 3d transition metals; in addition, an analysis of spectroscopic properties for ScH $^1\Sigma^+$, TiH $^4\Phi$, CrH $^4\Sigma^+$, CrH $^6\Sigma^+$, MnH $^5\Sigma^+$, MnH $^7\Sigma^+$, FeH $^4\Delta$, FeH $^6\Delta$, CoH $^3\Phi$, CuH $^1\Sigma^+$, and ZnH $^2\Sigma^+$.

2.2) **Computational Methods**

Calculations were completed using open-source quantum computational packages Psi4[22] and Forte. The package Forte was developed by our group and includes the software to complete perturbative MRDSRG calculations. Analysis of transition metal hydrides and atoms were completed using a nested approach with multiple computational techniques. Initially, experimental spectroscopic constants were obtained from databases compiled by Kulik et al.[4] and Aoto et al.[10] Utilizing experimental data, the constant a_o was calculated using a procedure developed by Dunham [23] that utilizes a rotating vibrator model to elucidate energy levels of diatomic molecules. The constant a_o is derived from a power series expansion of the Morse potential around the equilibrium bond distance r_e (Equation 29).

$$V = h\,c\,a_o\xi^2(1 + a_1\xi + a_2\xi^2 + a_3\xi^3 + \cdots) \tag{29}$$

Where $\xi = \frac{r-r_e}{r_e}$, h is Planck's constant, and c is the speed of light. For our purposes, we utilize Equation 1 when r = r_e and $\xi = 0$. In addition, a_o is the initial value of the power expansion and describes the width of the potential energy curve and was calculated via experimental data using the classical frequency, ω_e and the constant $B_e = \frac{h}{8\pi^2 m\, r_e^2\, c}$ where m is the reduced mass; then, $a_o = \frac{\omega_e^2}{4B_e}$.

Using the constant a_o, a potential energy curve was complete with points concentrated around the width of the potential energy curve as described by Aoto.[10] Every calculation was completed with at least a triple-zeta basis and employed either an aug-cc-pVnZ or cc-pVnZ (where n= T or Q).[19] The potential energy curve scan starts with a restricted or restricted open-

shell Hartree-Fock (RHF or ROHF) calculation in Psi4, followed by a CASSCF calculation and then a MRDSRG-PT2 or MRDSRG-PT3 calculation in Forte at the experimental r_e using AVAS (Atomic Valence Active Space) orbitals. A user selected active space of the 4s, 4p, and 3d atomic orbitals of the 3d transition metal and the 1s atomic orbital of hydrogen was chosen for the construction of the active space. Using the wavefunction of the initial calculation, the potential energy curve starts at a value of r=1Å, and proceeds throughout the curve using the previous wavefunction of the previous r value. In the center of the potential energy curve, the points are spaced closely together and based on the obtained constant of a_o.[10] Once the potential energy curve is obtained spectroscopic constant are ascertained using closely spaced points based on a_o using the anharmonicity driver within Psi4. The chosen points around a_o for every analyzed transition metal hydride are described in Table 1. Anharmonicity driver fits the given points using a weighted least squares approach which gives points closest to r_e the greatest statistical significance and was published by Bender and coworkers.[24] The calculation process is described in Figure 8.

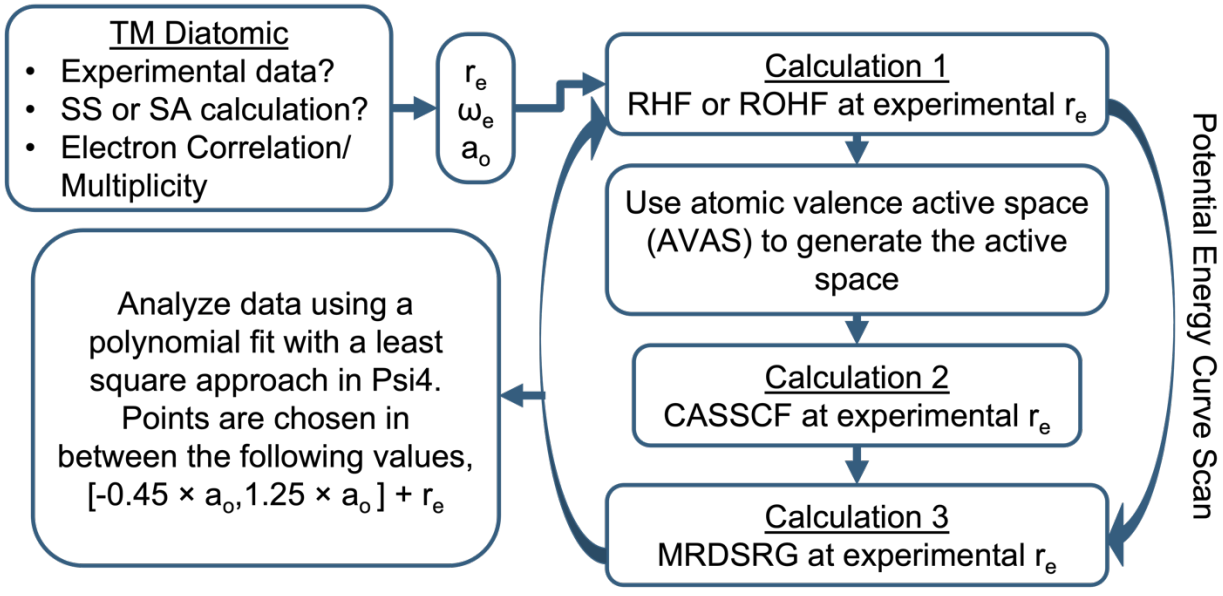

Figure 8. Flow chart of computational steps in the analysis of 3*d* transition metal atoms and hydrides.

After obtaining the spectroscopic constants using Psi4 the dissociation energy (D_e) was found by completing identical calculations for each 3d transition metal and an additional ROHF calculation for a hydrogen atom. Then ascertained results were applied to Equation 29 using the energy at the equilibrium bond distance of the transition metal hydride ($E(r_e)$) obtained via the polynomial fit, the energy of the transition metal atom $E(TM)$, and the energy of the hydrogen atom $E(H)$.

$$TM - H \rightarrow TM + H \tag{30}$$

$$[E(TM) + E(H)] - E(r_e) \tag{31}$$

The identical process was completed for 3d transition metal atoms to yield the first ionization energies with the chemical process described by Equation 32. In Equation 32, the variable X and e are defined as the transition metal atom of interest and the electron, respectively.

$$X \rightarrow X^+ + e \tag{32}$$

A user selected active space of the 4s, 4p, and 3d atomic orbitals of the 3d transition metal were chosen for the construction of the active space for the cation and neutral atom. Ionization energy was ascertained by completing a calculation using the process dictated in Figure 8 for the energy of cation ($E(X^+)$) and neutral atom ($E(X)$). Then Equation 33 was applied to obtain the first ionization energy (IE).

$$IE = E(X^+) - E(X) \tag{33}$$

Table 1. The bond distances in Å used to determine the spectroscopic constants for the 3d transition metal hydrides.

ScH $^1\Sigma^+$	1.7000, 1.7167, 1.7402, 1.7519, 1.7637, 1.7754, 1.7871, 1.7989, 1.8000, 1.8106, 1.8341, 1.8634, 1.9000, 1.9221
TiH $^4\Phi$	1.7000, 1.7180, 1.7416, 1.7534, 1.7652, 1.7770, 1.7888, 1.8000, 1.8006, 1.8124, 1.8360, 1.8655, 1.9000, 1.924
CrH $^4\Sigma^+$	1.6000, 1.6003, 1.6223, 1.6334, 1.6444, 1.6554, 1.6664, 1.6774, 1.6885, 1.7000, 1.7105, 1.7381, 1.7932
CrH $^6\Sigma^+$	1.5000, 1.6000, 1.6003, 1.6223, 1.6334, 1.6444, 1.6554, 1.6664, 1.6774, 1.6885, 1.7105, 1.7381, 1.7932, 1.8000, 1.9000
MnH $^5\Sigma^+$	1.5000, 1.6000, 1.6003, 1.6223, 1.6334, 1.6444, 1.6554, 1.6664, 1.6774, 1.6885, 1.7105, 1.7381, 1.7932
MnH $^7\Sigma^+$	1.6000, 1.6003, 1.6223, 1.6334, 1.6444, 1.6554, 1.6664, 1.6774, 1.6885, 1.7000, 1.7105, 1.7381, 1.7932, 1.8000, 1.9000
FeH $^4\Delta$	1.3000, 1.4000, 1.5000, 1.5425, 1.5679, 1.5806, 1.5933, 1.6000, 1.6060, 1.6187, 1.6314, 1.6441, 1.6695, 1.7000, 1.7013, 1.7648, 1.8000, 1.9000
FeH $^6\Delta$	1.5425, 1.5679, 1.5806, 1.5933, 1.6000, 1.6060, 1.6187, 1.6314, 1.6441, 1.6695, 1.7000, 1.7013, 1.7648, 1.8000, 1.9000
CoH $^3\Phi$	1.3000, 1.4000, 1.4688, 1.4943, 1.5000, 1.5071, 1.5199, 1.5327, 1.5455, 1.5583, 1.5711, 1.5966, 1.6000, 1.6286, 1.6925, 1.7000
CuH $^1\Sigma^+$	1.3000, 1.4000, 1.4033, 1.4270, 1.4389, 1.4507, 1.4626, 1.4745, 1.4863, 1.4982, 1.5000, 1.5219, 1.5515, 1.6000, 1.6107
ZnH $^2\Sigma^+$	1.5000, 1.5456, 1.5647, 1.5743, 1.5839, 1.5935, 1.6000, 1.6031, 1.6127, 1.6223, 1.6415, 1.6656, 1.7000, 1.7136

2.3) **First Ionization Energies**

The ionization energy of the 3d transition metals were calculated using MRDSRG-PT2 and MRDSRG-PT3 (Table 2 and Figure 9). Calculations were completed with larger augmented basis sets to accurately account for the valence electron correlation.[19] Thus, perturbative MRDSRG calculations were performed with an aug-cc-pVnZ basis set where n=T or Q. A flow parameter (s) of 0.5 E_h^{-2} was utilized to compule all ionization energies. Perturbative MRDSRG calculations were compared to experimental values reported in the NIST Chemical Webbook,[25] and calculated CCSD and CCSD(T) results by Balabanov and coworker.[26]

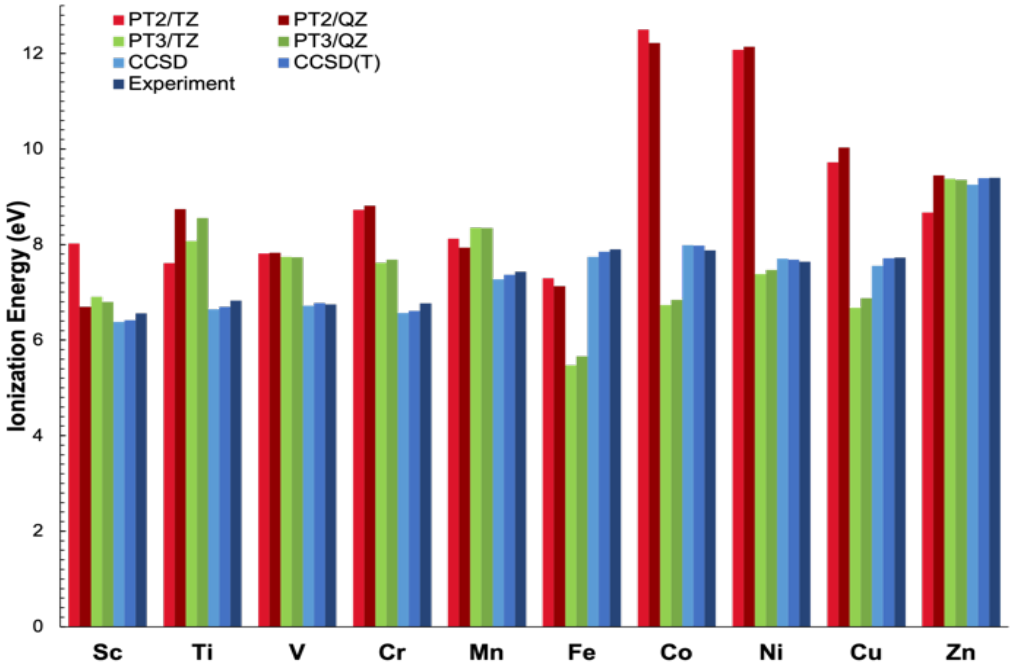

Figure 9. A visual representation of Table 2. The first ionization energies for calculations performed at the MRDSRG-PTx/aug-cc-pVnZ where x=2 or 3 and n=T or Q at s=0.5 E_h^{-2} are included. Additionally, CCSD and CCSD(T) calculations reported by Balabanov et al. and experimental results are presented.

Figure 9 demonstrates the performance of MRDSRG-PT2 and MRDSRG-PT3 for determining first ionization energies. Overall, calculations performed at the MRDSRG-PT3/aug-cc-pVQZ level of theory yielded results closer to experiment. Furthermore, calculated ionization energy for Zn with perturbative MRDSRG yielded results closest to the experimental value compared to other transition metals. The closed-shell nature of neutral Zn reduces the

possibility of inaccurate results for computational analysis. In addition, CCSD and CCSD(T) results completed by Balabanov and coworker[26] were similar to results obtained by perturbative MRDSRG for Zn.

Table 2. Compiled ionization energies in eV for 3d transition metals. Calculations were performed using an aug-cc-pVnZ basis set where n=T or Q with MRDSRG-PT2 and MRDSRG-PT3 using s=0.5 E_h^{-2}. Generated data is compared to CCSD and CCSD(T) in the complete basis set limit (CBS) and experimental results.

	MRDSRG-PT2		**MRDSRG-PT3**		**CCSD/CBS[a]**	**CCSD(T)/ CBS[a]**	**Experimental Results [b]**
	aug-cc-pVTZ	**aug-cc-pVQZ**	**aug-cc-pVTZ**	**aug-cc-pVQZ**	**aug-cc-pVnZ-DK, n=T, Q, 5**	**aug-cc-pVnZ-DK, n=T, Q, 5**	
Sc	8.03	6.70	6.91	6.80	6.38	6.41	6.56144
Ti	7.61	8.74	8.07	8.55	6.65	6.70	6.8282
V	7.81	7.83	7.74	7.73	6.72	6.78	6.746
Cr	8.73	8.81	7.62	7.69	6.57	6.61	6.76664
Mn	8.12	7.93	8.35	8.35	7.28	7.36	7.43402
Fe	7.30	7.13	5.47	5.66	7.74	7.85	7.9024
Co	12.50	12.22	6.74	6.84	7.99	7.98	7.881
Ni	12.08	12.14	7.38	7.47	7.71	7.68	7.6398
Cu	9.72	10.03	6.68	6.88	7.55	7.71	7.72638
Zn	8.67	9.45	9.38	9.35	9.25	9.39	9.39405

a: reference 26
b: reference 25

Perturbative MRDSRG calculations varied more from experimental as the atom exhibited less closed-shell behavior. For example, neutral Sc has only a single electron in the 3d orbital leading to fewer Slater determinants needed in the active space. Thus, perturbative MRDSRG obtains results close to experimental results, with MRDSRG-PT3 calculations being the closest to experiment for Sc.

However, in the middle of the periodic table results from perturbative MRDSRG yields results farther from the experimental value. Significant discrepancies between the experimental

value and perturbative MRDSRG is observed for Fe. The most difficult 3d transition metals to study with theoretical techniques are Fe, Co, and Ni.[4] The challenge of studying these transition metal atoms or complexes is due to the electron correlation present in Fe, Co and Ni. The number of possible electron configurations and thus Slater determinants in the wavefunction is greater for these atoms that exhibit a higher degree of open-shell character. When examining the 3d orbital of the Co atom in Figures 1 and 2 a total of 10 determinants where needed to describe a single spin-multiplicity of Co while neglecting spin. The sheer number of determinants and the significant open-shell behavior causes strong electron correlation to arise leading to inaccuracies in the computational method. Despite the significant amount of electron correlation predicted for Ni, MRDSRG-PT3 ascertained close results to experiment. Ni has 8 electrons within the 3d orbital and therefore would have more electron configuration than a transition metal like Zn with a filled 3d orbital and 4s orbital, or Mn with a half-filled 3d orbital and filled 4s orbital. The results yielded by MRDSRG-PT3 for Sc, Ni and Zn demonstrate that this method can be utilized to obtain ionization energies of 3d transition metals.

The quality of MRDSRG-PT3 calculations can be improved in several ways. The utilized *s*-value of 0.5 E_h^{-2} could have been an inappropriate choice for the calculations performed. Calculations were not performed at higher and lower flow parameters and thus, its impact on results could not be elucidated. To determine an appropriate *s* value, a systematic analysis of the impact of *s* on the ionization energy for each transition metal would be desirable. Additionally, CCSD and CCSD(T) data generated by Balabanov and colleague[26] reported results for the complete basis set (CBS) limit. Overall, in the perturbative MRDSRG calculations the energy decreased between the TZ and QZ basis set; this decrease in energy generally corresponding to better agreement between experiment and theory. Thus, computing the CBS and choosing the appropriate *s* value could lead to higher quality MRDSRG-PT3 results.

2.4) **Analysis of the Flow Parameter**

In this section we examine how to choose the value of *s* in perturbative MRDSRG calculations. This can be determined by analyzing trends in obtained spectroscopic constants. The best choice of *s* would ensure that enough electron correlation is introduced, spectroscopic constants do not exhibit major fluctuations with small changes in *s*, intruder states are accounted for, and calculations converge. If the value of *s* is too large calculations cannot converge and intruder states are reintroduced. On the other hand, if the value of *s* is too small the amount of electron correlation introduced is too small to accurately encapsulate the behavior for the system of interest.

Table 3. The dissociation energy in eV for different values of *s* using the MRDSRG-PT2 or MRDSRG-PT3 method with the cc-pVTZ or cc-pVQZ basis set.

s (E_h^{-2})	MRDSRG-PT2		MRDSRG-PT3	
	cc-pVTZ	cc-pVQZ	cc-pVTZ	cc-pVQZ
0	2.05	2.06	2.06	2.06
0.25	2.17	2.14	2.33	2.31
0.5	2.15	2.13	2.33	2.31
0.8	2.15	2.12	2.33	2.31
1	2.14	2.11	2.32	2.31
1.25	2.14	2.11	2.32	2.31
1.5	2.13	2.11	2.31	2.31
1.75	2.13	2.11	2.31	2.31
2	2.14	2.10	2.31	2.30
3	2.14	2.10	2.31	2.30
5	2.15	2.12	2.31	2.30
7	2.16	2.13	2.31	2.30
9	2.17	2.14	2.32	2.30

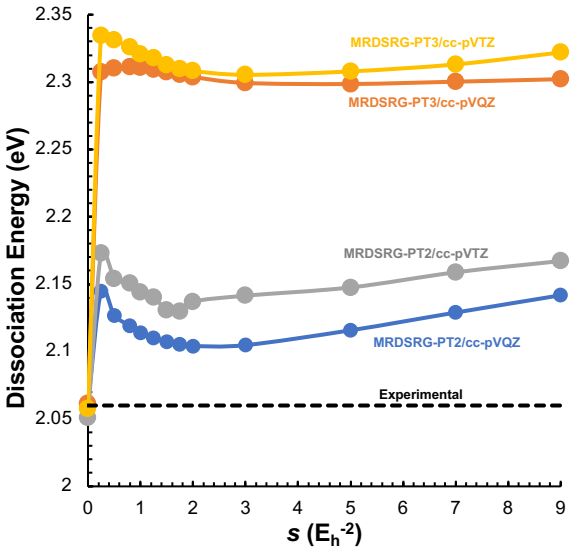

Figure 10. The dissociation energy in eV for plotted as a function of *s* using the MRDSRG-PT2 or MRDSRG-PT3 method with the cc-pVTZ or cc-pVQZ basis set. The experimental value is from reference 4.

To determine the best *s* value to be chosen for perturbative MRDSRG calculations for 3d transition metal hydrides an analysis of ScH $^1\Sigma^+$ was performed for $s \in [0, 9]$ E_h^{-2}. The following spectroscopic constants - dissociation energy (D_e), and equilibrium bond distance (r_e) were evaluated as a function of *s* at a MRDSRG-PTx/cc-pVnZ level of theory (where x=2 or 3, and n=T or Q). The value *s* where the spectroscopic constants varied the least was utilized for

calculations of ScH $^1\Sigma^+$, TiH $^4\Phi$, CrH $^4\Sigma^+$, CrH $^6\Sigma^+$, MnH $^5\Sigma^+$, MnH $^7\Sigma^+$, FeH $^4\Delta$, FeH $^6\Delta$, CoH $^3\Phi$, CuH $^1\Sigma^+$, and ZnH $^2\Sigma^+$.

Table 4. The equilibrium bond distance in Å. for different values of *s* using the MRDSRG-PT2 or MRDSRG-PT3 method with the cc-pVTZ or cc-pVQZ basis set.

s (E_h^{-2})	MRDSRG-PT2		MRDSRG-PT3	
	cc-pVTZ	cc-pVQZ	cc-pVTZ	cc-pVQZ
0	1.802	1.803	1.802	1.803
0.25	1.772	1.764	1.765	1.757
0.5	1.774	1.766	1.766	1.758
0.8	1.775	1.767	1.766	1.758
1	1.776	1.768	1.766	1.758
1.25	1.777	1.769	1.766	1.758
1.5	1.778	1.769	1.766	1.758
1.75	1.778	1.770	1.766	1.759
2	1.778	1.770	1.766	1.759
3	1.780	1.771	1.766	1.759
5	1.782	1.771	1.767	1.759
7	1.784	1.772	1.767	1.760
9	1.785	1.772	1.768	1.760

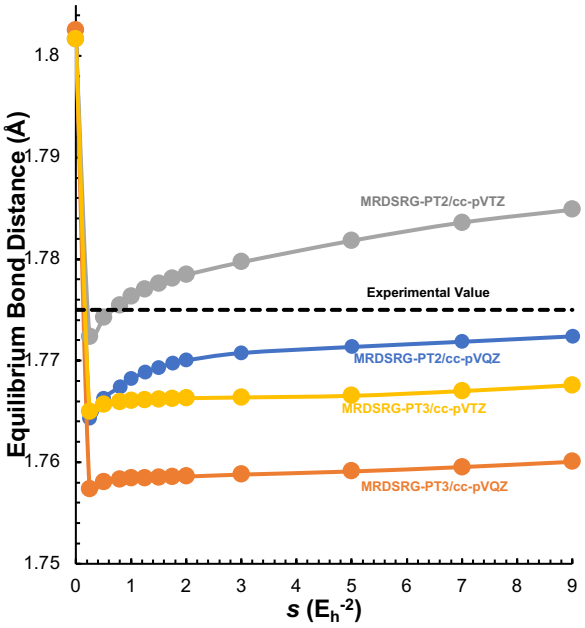

Figure 11. The equilibrium bond distance in Å plotted as a function of *s* using the MRDSRG-PT2 or MRDSRG-PT3 method with the cc-pVTZ or cc-pVQZ basis set. The experimental value is from reference 4.

In Figure 10 the dissociation energy as a function of *s* is shown and the corresponding values are tabulated in Table 3. The dissociation energy varied the least for when $s \in [1.5, 3.0]$ E_h^{-2} and $s \in [2.0, 3.5]$ E_h^{-2} for MRDSRG-PT2 and MRDSRG-PT3 respectively. At s=0 the Hamiltonian is not block-diagonalized and no electron correlation is introduced, therefore the dissociation energy is equivalent to the CASSCF energy. As the value of *s* is increased, electron correlation is introduced. Initially, the dissociation energy increases, which is expected since low values of *s* do not fully capture the electron correlation present in the system. Then for MRDRG-PT2 a very clear plateau is reached between $s \in [1.5, 3.0]$ E_h^{-2} for the cc-pVTZ and cc-pVQZ basis sets. Additionally, a less pronounced plateau is observed for MRDSRG-PT3 for $s \in [2.0, 3.5]$ E_h^{-2}. These plateaus are considered the range that the predicted "sweet spot" is since, the dissociation energy does not remarkably vary. Furthermore, the plateaus are followed by an

increase in dissociation energy. MRDSRG-PT2 showcased the most significant increase in dissociation energy after the plateau is reached. MRDSRG-PT3 demonstrated a small increase in dissociation energy that was more prevalent for the cc-pVTZ basis. The increase after the predicted "sweet spot" is reached suggests that intruder states are reintroduced as the value of *s* increases past the "sweet spot."

An analysis of the equilibrium bond distance and the *s* value was also conducted (Figure 11 and Table 4). However, the observed relationship between the equilibrium bond distance and the s-value was less significant. The CASSCF equilibrium bond distance at s=0 E_h^{-2} is significantly greater than the experimental value. Then, as electron correlation is introduced, the equilibrium bond distance significantly decreases and is closer to the experimental value for the MRDSRG-PT2 data. Overall, the equilibrium bond distance stays relatively constant between $s \in [0.25, 9.0]$ E_h^{-2}. This result suggests that the equilibrium bond distance is not as sensitive to *s* as the dissociation energy.

Therefore, the "sweet spot" determined for the dissociation energy was considered for further transition metal hydride calculations. These preliminary calculations ascertained results closer to experiment for the MRDSRG-PT2 than MRDSRG-PT3. Nonetheless, the dissociation energy and the equilibrium bond distance varied the least as a function of *s* for the MRDSRG-PT3 theory compared to the MRDSRG-PT2 theory. Additionally, calculations in this section were completed using a non-augmented basis set. Calculations completed in Section 2.3 determined that MRDSRG-PT3 with an augmented basis set ascertained values for the first ionization energies of 3d transition metals closer to experiment than MRDSRG-PT2. Thus, the evaluation of spectroscopic constants for ScH $^1\Sigma^+$, TiH $^4\Phi$, CrH $^4\Sigma^+$, CrH $^6\Sigma^+$, MnH $^5\Sigma^+$, MnH $^7\Sigma^+$, FeH $^4\Delta$, FeH $^6\Delta$, CoH $^3\Phi$, CuH $^1\Sigma^+$, and ZnH $^2\Sigma^+$ were completed at a value of s=2.5 E_h^{-2} at the MRDSRG-PT3/aug-cc-pVnZ (n=T, Q) level of theory.

2.5) **Analysis of 3d Transition Metal Hydrides**

This section reports an analysis of 3d transition metal hydrides. Based on the results presented in Section 2.4, the calculations of 3d transition metal hydrides were completed utilizing MRDSRG-PT3 with an aug-cc-pVTZ or aug-cc-pVQZ basis set at a value of s=2.5 E_h^{-2}. The dissociation energy (D_e), equilibrium bond distance (r_e), and equilibrium frequency (ω_e) were computed for ScH $^1\Sigma^+$, TiH $^4\Phi$, MnH $^5\Sigma^+$, MnH $^7\Sigma^+$, and ZnH $^2\Sigma^+$. The equilibrium bond lengths for ScH $^1\Sigma^+$, TiH $^4\Phi$, CrH $^4\Sigma^+$, CrH $^6\Sigma^+$, MnH $^5\Sigma^+$, MnH $^7\Sigma^+$, FeH $^4\Delta$, FeH $^6\Delta$, CoH $^3\Phi$, CuH $^1\Sigma^+$, and ZnH $^2\Sigma^+$ and the energy splitting observed between MnH $^5\Sigma^+$ and MnH $^7\Sigma^+$ were also determine.

Table 5 shows the obtained spectroscopic properties for ScH $^1\Sigma^+$, TiH $^4\Phi$, MnH $^5\Sigma^+$, MnH $^7\Sigma^+$, and ZnH $^2\Sigma^+$. The larger aug-cc-pVQZ basis set yielded results closer to experimental values than the aug-cc-pVTZ, basis set yielding similar results to Balabanov and coworker's basis set analysis of 3d transition metals.[19] Furthermore, MRDSRG-PT3 yields results close to experiment for equilibrium bond distances, in accordance with other techniques reported in Table 5. Compared to icMRCCSD(T) calculation performed by Aoto et al.,[10] dissociation energies and equilibrium bond distances are comparable to this higher level of theory. For MnH $^7\Sigma^+$ the dissociation energy is overestimated for MRDSRG-PT3/aug-cc-pVQZ (1.72 eV), GGA (1.75 eV),[4] CCSD(T) (1.65 eV)[10] and icMRCCSD(T) (1.71 eV)[10] compared to the experiment (1.35 eV). MnH $^5\Sigma^+$ and MnH $^7\Sigma^+$ are extensively prone to sensitivities in electron correlation due to the significant number of possible electron configurations. The DFT calculations by Kulik and colleagues[4] completed with the GGA functional that does not account for strong electron correlation and significantly overestimates the dissociation energy compared to GGA+U (1.38 eV). However, the overestimation of the multireference techniques (including MRDSRG-PT3 and excluding MRCI) indicates that the weak electron correlation is not completely accounted for by these techniques for MnH $^7\Sigma^+$. Additionally, complete potential energy curves were obtained for ScH $^1\Sigma^+$, TiH $^4\Phi$, and ZnH $^2\Sigma^+$ indicating that intruder states were not introduced in

the performed MRDSRG-PT3 calculations (Figure 12, Figure 13 and Figure 14). Potential energy curves also suggest that the selection of active space via AVAS was successful. Overall, MRDSRG-PT3 was able to yield data close to experiment for the dissociation energies and the equilibrium bond distances for the analyzed transition metal hydrides.

Table 5. Obtained spectroscopic constants for different computational methods and the corresponding basis set.

		MRDSRG-PT3 s=2.5 E_h^{-2}		GGA[a]	GGA+$U_{3d/4s}$[a]	MRCI[a]	CCSD(T)[b]	icMRCCSD(T)[b]	Experiment[a,b]
		aug-cc-pVTZ	aug-cc-pVQZ	6-311++G			awCVTZ(-PP)		
ScH	r_e (Å)	1.764	1.757	1.760	1.783	1.787	1.767	1.796	1.775
	ω_e (cm^{-1})	1634	1613	1603	1596	1589	1607	1567	1547
$^1\Sigma^+$	D_e (eV)	2.35	2.35	2.59	2.04	2.06	2.26	2.38	2.06
TiH	r_e (Å)	1.804	1.793	···	···	···	1.774	1.806	1.777
	ω_e (cm^{-1})	1539	1587	···	···	···	1555	1517	1567
$^4\Phi$	D_e (eV)	2.00	2.07	···	···	···	2.10	2.25	2.06
MnH	r_e (Å)	1.632	1.620	1.592	1.617	1.662	···	···	1.605
	ω_e (cm^{-1})	1623	1672	1729	1692	1565	···	···	1720
$^5\Sigma^+$	D_e (eV)	1.51	1.58	1.84	1.66	1.59	···	···	···
MnH	r_e (Å)	1.732	1.718	1.714	1.725	1.744	1.737	1.748	1.731
	ω_e (cm^{-1})	1608	1640	1546	1527	1580	1546	1543	1548
$^7\Sigma^+$	D_e (eV)	1.64	1.72	1.75	1.38	1.25	1.65	1.71	1.35
ZnH	r_e (Å)	1.552	1.551	1.605	1.609	1.586	1.604	1.603	1.594
	ω_e (cm^{-1})	1844	1926	1543	1503	1767	1607	1626	1603
$^2\Sigma^+$	D_e (eV)	1.11	0.70	1.05	0.95	1.04	0.96	1.00	1.01

a: reference 4
b: reference 10

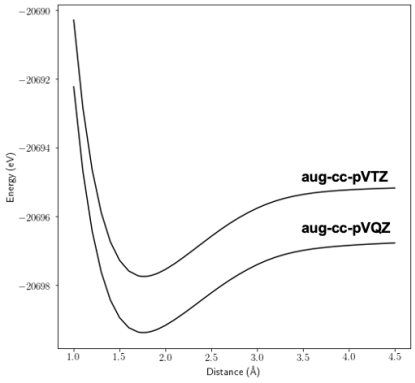

Figure 12. ScH $^{1}\Sigma^{+}$ potential energy curve generated via MRDSRG-PT3.

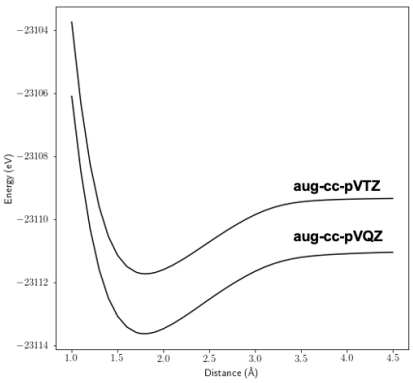

Figure 13. TiH $^{4}\Phi$ potential energy curve generated via MRDSRG-PT3.

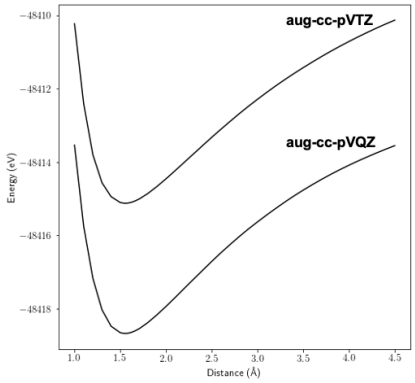

Figure 14. ZnH $^{2}\Sigma^{+}$potential energy curve generated via MRDSRG-PT3.

Additional analysis of equilibrium bond distances for an extended list of transition metal hydrides was completed for ScH $^{1}\Sigma^{+}$, TiH $^{4}\Phi$, CrH $^{4}\Sigma^{+}$, CrH $^{6}\Sigma^{+}$, MnH $^{5}\Sigma^{+}$, MnH $^{7}\Sigma^{+}$, FeH $^{4}\Delta$, FeH $^{6}\Delta$, CoH $^{3}\Phi$, CuH $^{1}\Sigma^{+}$, and ZnH $^{2}\Sigma^{+}$ (Table 6). In general, MRDSRG-PT3 predicts equilibrium bond distances close to experimental values and the additional computation techniques evaluated in Table 6. The mid-row transition metal hydrides or CrH, MnH, and FeH are considered the most challenging to study with theory.[4] They are also the transition metal hydrides for which the equilibrium bond distance was calculated for two states. Experimentally, CrH $^{6}\Sigma^{+}$, MnH $^{7}\Sigma^{+}$, and FeH $^{4}\Delta$ are the predicted ground states. Thus, for MRDSRG-PT3 to match experiment the obtained equilibrium bond distances for the predicted ground states should be less than the equilibrium bond distance for the excited states. In Table 6, the equilibrium bond length for FeH $^{4}\Delta$ is approximately 0.2 Å less than FeH $^{6}\Delta$ for the MRDSGR-PT3/aug-cc-pVQZ level of theory which is consistent with experiment. For CrH, MRDSRG-PT3/aug-cc-pVQZ overestimates the equilibrium bond distance for the sextet state, however, obtained results with the aug-cc-pVTZ basis set were consistent with experimental predictions. The most interesting case of energy splitting for the 3d transition metal hydrides is MnH. Although, the experimental equilibrium bond length is longer for the septet state compared to the quintet; experimental results predict MnH $^{7}\Sigma^{+}$ to be the ground state. In Table 6, ascertained

data for MnH for MRDSRG-PT3 provides good agreement with experimental data thus, the energy splitting was further examined.

Table 6. The equilibrium bond distance in Å for different computational methods and the corresponding basis set.

	MRDSRG-PT3 s=2.5 E_h^{-2}		GGA[a]	GGA+$U_{3d/4s}$[a]	MRCI[a]	CCSD(T)[b]	icMRCCSD(T)[b]	Experiment[a,b]
	aug-cc-pVTZ	aug-cc-pVQZ		6-311++G		awCVTZ(-PP)		
ScH $^1\Sigma^+$	1.764	1.757	1.760	1.783	1.787	1.767	1.796	1.775
TiH $^4\Phi$	1.804	1.793	···	···	···	1.774	1.806	1.777
CrH $^4\Sigma^+$	1.682	1.669	1.600	1.620	1.742	···	···	1.672
CrH $^6\Sigma^+$	1.664	1.745	1.650	1.668	1.678	1.640	1.667	1.655
MnH $^5\Sigma^+$	1.632	1.620	1.592	1.617	1.662	···	···	1.605
MnH $^7\Sigma^+$	1.732	1.718	1.714	1.725	1.744	1.737	1.748	1.731
FeH $^4\Delta$	1.512	1.525	1.560	1.587	1.583	1.560	1.580	1.589
FeH $^6\Delta$	1.678	1.724	1.670	1.701	1.690	···	···	1.770
CoH $^3\Phi$	1.496	1.506	···	···	···	1.525	1.517	1.533
CuH $^1\Sigma^+$	1.453	1.430	1.487	1.500	1.463	1.484	1.488	1.463
ZnH $^2\Sigma^+$	1.552	1.551	1.605	1.609	1.586	1.604	1.603	1.594

a: reference 4
b: reference 10

Lastly, we examine the energy splitting between the MnH $^5\Sigma^+$ and MnH $^7\Sigma^+$ states via MRDSRG-PT3 (Table 7). For both augmented basis sets the energy splitting yielded good agreement with experiment (0.21 eV). Furthermore, MRDSRG-PT3 performed similarly to the GGA+U and more closely matched experiment for MRCI calculation performed by Kulik et al.[4] In addition, potential energy curves were obtained for MnH $^5\Sigma^+$ and MnH $^7\Sigma^+$ using MRDSRG-PT3 with a aug-cc-pVQZ basis set (Figure15). Figure 15 shows that MnH $^7\Sigma^+$ is the lowest energy state across the entire potential energy curve.

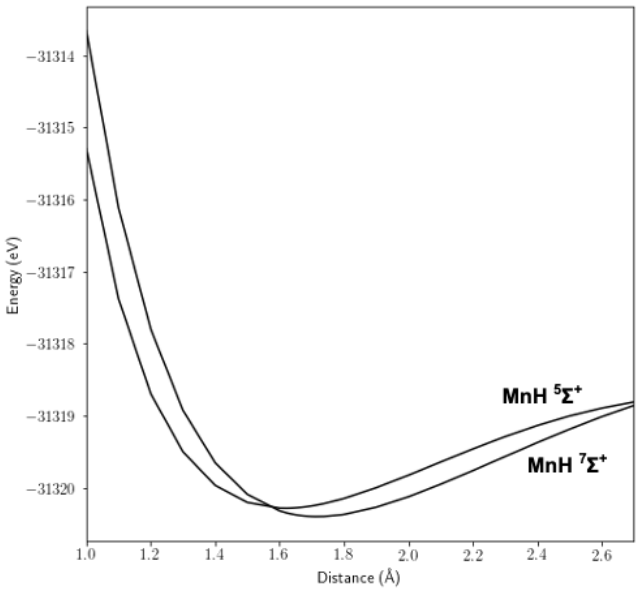

Figure 15. Potential energy curves for MnH $^7\Sigma^+$ and MnH $^5\Sigma^+$ at the MRDSRG-PT3/aug-cc-pVQZ level of theory.

Table 7. Energy splitting for MnH $^7\Sigma^+ \rightarrow {}^5\Sigma^+$ in eV generated via MRDSRG-PT3 compared to other computational methods.

MRDSRG-PT3 s=2.5 E_h^{-2}		GGA[a]	GGA+$U_{3d/4s}$[a]	MRCI[a]	Experiment[a]
aug-cc-pVTZ	aug-cc-pVQZ		6-311++G		
0.20	0.19	0.01	0.21	0.30	0.21

a: reference 4

Chapter 3 Conclusion

The study of transition metal chemistry has broad-ranging societal chemical relevance including biological processes such as oxygen-transport by iron-complexes, providing catalysts for industrial reactions, and materials for advancing solar cell development. However, computational methods currently presented in the literature have shortcomings in describing transition metal complexes. This analysis utilized perturbative MRDSRG to analyze 3d transition metal hydrides and calculate the ionization energies for 3d transition metals. Data presented in this report demonstrate that MRDSRG-PT3 can be utilized as an effective tool to understand 3d transition metal chemistry. The MRDSRG-PT3/aug-cc-pVQZ level of theory was able to predict equilibrium bond distances that agree with experimental values for a range of 3d transition metal hydrides, correctly predict the ground state for the complicated case of MnH $^{5}\Sigma^{+}$ and MnH $^{7}\Sigma^{+}$, generate potential energy curves for ScH $^{1}\Sigma^{+}$, TiH $^{4}\Phi$, and ZnH $^{2}\Sigma^{+}$, and obtain first ionization energies for 3d Sc, Ni, and Zn. This report presents an initial starting point that can be utilized study the chemistry of 3d transition metals with the MRDSRG-PT3 method.

References

(1) Beaumier, E. P.; Pearce, A. J.; See, X. Y.; Tonks, I. A. Modern Applications of Low-Valent Early Transition Metals in Synthesis and Catalysis. *Nat. Rev. Chem.* **2019**, *3* (1), 15–34. https://doi.org/10.1038/s41570-018-0059-x.

(2) Shon, J.-H.; Teets, T. S. Molecular Photosensitizers in Energy Research and Catalysis: Design Principles and Recent Developments. *ACS Energy Lett.* **2019**, *4* (2), 558–566. https://doi.org/10.1021/acsenergylett.8b02388.

(3) Pony Yu, R.; Hesk, D.; Rivera, N.; Pelczer, I.; Chirik, P. J. Iron-Catalysed Tritiation of Pharmaceuticals. *Nature* **2016**, *529* (7585), 195–199. https://doi.org/10.1038/nature16464.

(4) Kulik, H. J.; Marzari, N. Systematic Study of First-Row Transition-Metal Diatomic Molecules: A Self-Consistent DFT+U Approach. *J. Chem. Phys.* **2010**, *133* (11), 114103. https://doi.org/10.1063/1.3489110.

(5) Stevens, A. E.; Feigerle, C. S.; Lineberger, W. C. Laser Photoelectron Spectroscopy of MnH^- and FeH^-: Electronic Structures of the Metal Hydrides, Identification of a Low-spin Excited State of MnH, and Evidence for a Low-spin Ground State of FeH. *J. Chem. Phys.* **1983**, *78* (9), 5420–5431. https://doi.org/10.1063/1.445470.

(6) Szabo, A.; Ostlund, N. S. *Modern Quantum Chemistry: Introduction to Advanced Electronic Structure Theory*; Dover Publications.

(7) Evangelista, F. A. Perspective: Multireference Coupled Cluster Theories of Dynamical Electron Correlation. *J. Chem. Phys.* **2018**, *149* (3), 030901. https://doi.org/10.1063/1.5039496.

(8) Feller, D.; Peterson, K. A.; Dixon, D. A. A Survey of Factors Contributing to Accurate Theoretical Predictions of Atomization Energies and Molecular Structures. *J. Chem. Phys.* **2008**, *129* (20), 204105. https://doi.org/10.1063/1.3008061.

(9) Moltved, K. A.; Kepp, K. P. The Metal Hydride Problem of Computational Chemistry: Origins and Consequences. *J. Phys. Chem. A* **2019**, *123* (13), 2888–2900. https://doi.org/10.1021/acs.jpca.9b02367.

(10) Aoto, Y. A.; de Lima Batista, A. P.; Köhn, A.; de Oliveira-Filho, A. G. S. How To Arrive at Accurate Benchmark Values for Transition Metal Compounds: Computation or Experiment? *J. Chem. Theory Comput.* **2017**, *13* (11), 5291–5316. https://doi.org/10.1021/acs.jctc.7b00688.

(11) Xu, X.; Zhang, W.; Tang, M.; Truhlar, D. G. Do Practical Standard Coupled Cluster Calculations Agree Better than Kohn–Sham Calculations with Currently Available Functionals When Compared to the Best Available Experimental Data for Dissociation Energies of Bonds to 3 *d* Transition Metals? *J. Chem. Theory Comput.* **2015**, *11* (5), 2036–2052. https://doi.org/10.1021/acs.jctc.5b00081.

(12) Johnson, E. R.; Becke, A. D. Communication: DFT Treatment of Strong Correlation in 3d Transition-Metal Diatomics. *J. Chem. Phys.* **2017**, *146* (21), 211105. https://doi.org/10.1063/1.4985084.

(13) Hohenstein, E. G.; Luehr, N.; Ufimtsev, I. S.; Martínez, T. J. An Atomic Orbital-Based Formulation of the Complete Active Space Self-Consistent Field Method on Graphical Processing Units. *J. Chem. Phys.* **2015**, *142* (22), 224103. https://doi.org/10.1063/1.4921956.

(14) Chaban, G.; Schmidt, M. W.; Gordon, M. S. Approximate Second Order Method for Orbital Optimization of SCF and MCSCF Wavefunctions. *Theor. Chem. Acc. Theory Comput. Model. Theor. Chim. Acta* **1997**, *97* (1–4), 88–95. https://doi.org/10.1007/s002140050241.

(15) Sayfutyarova, E. R.; Sun, Q.; Chan, G. K.-L.; Knizia, G. Automated Construction of Molecular Active Spaces from Atomic Valence Orbitals. *J. Chem. Theory Comput.* **2017**, *13* (9), 4063–4078. https://doi.org/10.1021/acs.jctc.7b00128.

(16) Knizia, G. Intrinsic Atomic Orbitals: An Unbiased Bridge between Quantum Theory and Chemical Concepts. *J. Chem. Theory Comput.* **2013**, *9* (11), 4834–4843. https://doi.org/10.1021/ct400687b.

(17) Li, C.; Evangelista, F. A. Multireference Theories of Electron Correlation Based on the Driven Similarity Renormalization Group. **2019**, 31.
(18) Evangelista, F. A. A Driven Similarity Renormalization Group Approach to Quantum Many-Body Problems. *J. Chem. Phys.* **2014**, *141* (5), 054109. https://doi.org/10.1063/1.4890660.
(19) Balabanov, N. B.; Peterson, K. A. Systematically Convergent Basis Sets for Transition Metals. I. All-Electron Correlation Consistent Basis Sets for the 3d Elements Sc–Zn. *J. Chem. Phys.* **2005**, *123* (6), 064107. https://doi.org/10.1063/1.1998907.
(20) Lodi, L.; Yurchenko, S. N.; Tennyson, J. The Calculated Rovibronic Spectrum of Scandium Hydride, ScH. *Mol. Phys.* **2015**, *113* (13–14), 1998–2011. https://doi.org/10.1080/00268976.2015.1029996.
(21) Johnson, E. R.; Becke, A. D. Communication: DFT Treatment of Strong Correlation in 3d Transition-Metal Diatomics. *J. Chem. Phys.* **2017**, *146* (21), 211105. https://doi.org/10.1063/1.4985084.
(22) Psi4: An Open-source Ab Initio Electronic Structure Program. *Softw. Focus* **2011**, *2*, 10.
(23) Dunham, J. L. The Energy Levels of a Rotating Vibrator. *Phys. Rev.* **1932**, *41* (6), 721–731. https://doi.org/10.1103/PhysRev.41.721.
(24) Bender, J. D.; Doraiswamy, S.; Truhlar, D. G.; Candler, G. V. Potential Energy Surface Fitting by a Statistically Localized, Permutationally Invariant, Local Interpolating Moving Least Squares Method for the Many-Body Potential: Method and Application to N_4. *J. Chem. Phys.* **2014**, *140* (5), 054302. https://doi.org/10.1063/1.4862157.
(25) *NIST Chemistry WebBook*; 69; National Institute of Standards and Technology: Gaithersburg MD.
(26) Balabanov, N. B.; Peterson, K. A. Basis Set Limit Electronic Excitation Energies, Ionization Potentials, and Electron Affinities for the 3d Transition Metal Atoms: Coupled Cluster and Multireference Methods. *J. Chem. Phys.* **2006**, *125* (7), 074110. https://doi.org/10.1063/1.2335444.